Electronic Supplementary Material (ESI) for CrystEngComm.

Unravelling Substitution Effects on Charge Transfer Characteristics in Cocrystals of Pyrene Based Donors and 3,5-Dinitrobenzoic Acid

Arkalekha Mandal,[a] Kari Rissanen,[b*] Prasenjit Mal[a*]

[a]School of Chemical Sciences, National Institute of Science Education and Research (NISER), HBNI, Bhubaneswar, PO Bhimpur-Padanpur, District Khurda, Odisha 752050, India

[b]University of Jyvaskyla, Department of Chemistry, P.O. Box 35, Jyväskylä, FIN-40014, Finland.

E-mail: pmal@niser.ac.in , kari.t.rissanen@jyu.fi

EXPERIMENTAL SECTION

Syntheses of cocrystals 1-3

Synthesis of pyrene:3,5-dinitrobenzoic acid ·1,4-dioxane (1, CCDC: 1576743): Pyrene (20 mg, 1 mmol) and 3,5-dinitrobenzoic acid (21 mg, 1 mmol) were grinded together and few drops of methanol was added subsequently. Bright yellow colour appears on adding methanol indicating charge transfer. The mixture was grinded thoroughly with addition of four/ five drops of methanol at regular intervals for five minutes. The resultant yellow solid was dissolved in 1,4-dioxane and needle shaped yellow crystals were obtained after a week.

Synthesis of 1-aminopyrene:3,5-dinitrobenzoic acid·DMF (2, CCDC: 1909045): Equimolar amounts of 1-aminopyrene (22 mg, 1 mmol) and 3,5-dinitrobenzoic acid (21 mg, 1 mmol) were grinded with few drops of methanol as stated above to produce brown solid. The brown solid was dissolved in DMF to produce block shaped brown crystals after a month.

Synthesis of 1-bromopyrene:3,5-dinitrobenzoic acid (3, CCDC: 1909046): Equimolar amounts of 1-bromopyrene (28 mg, 1 mmol) and 3,5-dinitrobenzoic acid (21 mg, 1 mmol) were grinded with assistance of methanol to produce canary yellow solid. The solid was dissolved in chloroform: hexane (2:1) to produce needle shaped yellow crystals after five days.

Table S1. Crystal structure and refinement of cocrystals **1-3**

	Cocrystal **1**	Cocrystal **2**	Cocrystal **3**
chem formula	$C_{25}H_{18}N_7O_2$	$C_{49}H_{37}N_7O_{13}$	$C_{39}H_{22}N_2O_6Br_2$
formula wt	458.41	931.85	774.40
CCDC Number	1576743	1909045	1909046
crystal system	Triclinic	Monoclinic	Triclinic
space group	P -1	C 1 2/ c 1	P -1
a (Å)	6.6108(5)	10.1503(3)	8.694(12)
b (Å)	9.5147(7)	11.2758(3)	10.2148(3)
c (Å)	17.1651(10)	35.8393(11)	17.2379(4)
α (°)	96.283(5)	90	99.498(2)
β (°)	95.365(5)	93.409(3)	90.396(2)
γ (°)	103.343(6)	90	97.114(2)
V (Å^3)	1036.32(12)	4094.6(2)	1497.68(7)
Z	2	4	2
F_{000}	476	1936	776
ρ_{calcd} (g cm^{-3})	1.469	1.512	1.717
μ	0.109	0.112	2.764
no. of unique rflns/ no. of rflns ($I \geq 2\sigma (I)$)	3703/ 2282	3610/ 2491	5260/4610
$R_1{}^a$/ $R_1{}^b$ (all data, $I \geq 2\sigma(I)$)	0.0995/ 0.0569	0.088/ 0.0567	0.0726/ 0.0640
$wR_2{}^a$/ $wR_2{}^b$ (all data, $I \geq 2\sigma(I)$)	0.1535/ 0.1309	0.1532/0.1308	0.1691/ 0.1625
goodness of fit (F^2)	0.978	1.047	1.120
largest peak/hole (e Å^{-3})	-0.266/ 0.241	-0.512/ 0.411	-0.828/ 1.327

Table S2. Parameters of weak interactions in cocrystals **1**, **2** and **3**

Cocrystal	Interaction	D···A (Å)	H···A (Å)	D−H···A (º)	Binding energy by M06-2X/6-311G(d,p) level (kcal/mol)
1	O−H···O	2.606(3)	1.596	176.45	-20.56
	C−H···nitro-O	3.624(3)	2.780	151.37	-1.92
	C−H···nitro-O	3.347(4)	2.643	133.00	
	C−H···nitro-O	3.523(3)	2.664	154.05	-1.30
	C−H···nitro-O	3.660(4)	2.593	163.08	-0.92
	C−H···diox-O	3.359(4)	2.456	163.88	-1.68
2	O1−H1···O2	2.622(4)	1.808	171.47	-12.22
	N1−H1A···nitro-O	3.322(4)	2.489	163.13	-3.13
	N1−H1A···nitro-O	3.270(4)	2.533	148.23	
	N1−H1B···DMF-O	3.266(4)	2.531	143.91	-7.05
	C−H···DMF-O	3.683()	2.763	169.94	
	C15−H15···nitro-O	3.470(4)	2.585	159.13	-1.35
	C9−H9···nitro-O	3.707(4)	2.810	162.24	
3	O−H···O	2.641(2)	1.834	167.51	-11.18
	C4B−H4BA···Br1	3.976(3)	3.098	158.06	
	C−H···O	3.445(2)	2.541	167.60	
	C−H···Br	3.940(4)	3.045	159.61	-2.37
	O···Br	2.972(3)			

Characterization

The solids were characterized using single crystal XRD, powder XRD, X-band EPR, FTIR and UV-Vis taken in both solid and solution. A Perkin Elmer Spectrum FTIR spectrometer (4000-250 cm^{-1}), Bruker X-band EPR, Bruker D8 Advance and Perkin Elmer Lambda 25 spectrometer were used for measurements. X-ray crystallographic data was collected using Bruker SMART APEX-CCD diffractometer with Mo-Kα radiation (λ= 0.71073 Å). Bulk phase purity of the cocrystals was confirmed by powder XRD. No characteristic charge transfer bands were observed in UV-Vis of cocrystal solution in chloroform: hexane (1:1). The optical bandgap of the cocrystals were calculated using modified Kubelka-Munk equation ($E = hc/\lambda = 1240/\lambda$) In contrast, all cocrystals exhibit characteristic broad charge transfer band in solid state UV-Vis spectra. IR spectra of all cocrystals in powder form were recorded using KBr palate.

Crystal refinement

The crystals data were collected with Bruker SMART D8 goniometer equipped with an APEX CCD detector and with an INCOATEC micro source (Cu-Kα radiation, λ = 0.71073 Å). SAINT+[1] and SADABS[2] were used to integrate the intensities and to correct the absorption respectively The structure was resolved by direct methods and refined on F^2 with SHELXL-97.[3]

Computational methods

Geometry optimization and HOMO/ LUMO energy calculation of the donor/ acceptor coformers was performed at B3LYP/6-311G(d,p) level of theory. Adiabatic ionization potential and electron affinities of the coformers were calculated by taking optimized geometries of the radical cation and anions in consideration. All theoretical calculations of the cocrystals were performed using crystal co-coordinates as the starting geometry using. HOMO, LUMO energies and static dipole moment (SDM) of the cocrystals were calculated employing DFT calculations at M06-2X/6-311G(d, p) level of theory to take account of the dispersive nature of $\pi\cdots\pi$ stacking.[4] Direct and super-exchange charge transfer integrals were calculated using orbital energies of dimmers and trimers obtained from crystal coordinates. Coulomb attenuated version of B3LYP (CAM-B3LYP) functional and 6-311G(d, p) basis set were used to calculate transfer integrals for accounting long range correction (LRC).[5] Wavelength, oscillator strength (f) and orbital contributions for vertical excitation were calculated by TD-DFT method using B3LYP/6-311G(d,p) level of theory on crystal geometries. Excitations in gas phase was calculated by TD-DFT method and compared with experimentally obtained UV-Vis in solid state. Magnetic transition dipole moments (TDM) were considered to ascertain charge transfer nature of electronic excitation. The interaction energies of different weak inetarctions were calculated at M06-2X/6-311G(d,p) level following basis set superposition error corrected (BSSE) method of Boys and Bernerdi to attain complete basis set (CBS) limit.[6]

Hirshfeld surface analyses

All intermolecular interactions in crystal structures of cocrystals **1**, **2** and **3** were analysed quantitatively using d_{norm} surface with 2D fingerprint plots.[7] The red, white and blue regions on the d_{norm} surface demonstrate respectively short range contacts, contacts at van der Waals separation and contacts with longer distance. Interaction energies of molecular dimers were calculated with energy decomposition analyses (EDA).[8] The total energy of an interaction is a summation of electrostatic, polarization, dispersion and repulsion energies. $E_{total} = k_{electric}E_{electric}+k_{polarization}E_{polarization}+k_{dispersion}E_{dispersion}+k_{repulsion}E_{repulsion}$, where k indicates all scaled factors. Accurate values of electrostatic, polarization and repulsion energies were obtained with B3LYP/6-31G(d,p) level of theory using Crystalexplorer 17.5 version. Values of scaled factors are listed below.

Table S3. Scaled factor (k) values for energy decomposition analyses (EDA) in **1-3**

Cocrystal	$k_{electric}$	$k_{polarization}$	$k_{dispersion}$	$k_{repulsion}$
1	1.019	0.611	0.901	0.851
2	1.019	0.651	0.901	0.811
3	1.018	0.620	0.903	0.810

Table S4. Contribution of weak interactions in crystal packing of cocrystals **1-3**

Cocrystal	Weak interaction	Contribution (%)
1	O···H	39.8
	C−H···π	5.7
	π···π	7.5
2	O···H	41.7
	C−H···π	8.4
	π···π	5.0

3	O···H	25.6
	O···Br	3.4
	C−H···π	4.6
	π···π	6.6
	C−H···Br	11.2

References

1. SAINT+, Bruker AXS Inc., Madison, Wisconsin, USA, 1999 (Program for Reduction of Data collected on Bruker CCD Area Detector Diffractometer V. 6.02.)
2. SADABS, Bruker AXS, Madison, Wisconsin, USA, 2004
3. Sheldrick, G., A short history of SHELX. *Acta Crystallogr. Sect. A* **2008,** *64*, 112-122.
4. Zhao, Y.; Truhlar, D. G., The M06 suite of density functionals for main group thermochemistry, thermochemical kinetics, noncovalent interactions, excited states, and transition elements: two new functionals and systematic testing of four M06-class functionals and 12 other functionals. *Theor. Chem. Acc.* **2007,** *120*, 215-241.
5. Pedone, A., Role of Solvent on Charge Transfer in 7-Aminocoumarin Dyes: New Hints from TD-CAM-B3LYP and State Specific PCM Calculations. *J. Chem. Theory Comput.* **2013,** *9*, 4087-4096.
6. Boys, S. F.; Bernardi, F., The calculation of small molecular interactions by the differences of separate total energies. Some procedures with reduced errors. *Mol. Phys.* **1970,** *19*, 553-566.
7. Spackman, M. A.; McKinnon, J. J., Fingerprinting intermolecular interactions in molecular crystals. *CrystEngComm* **2002,** *4*, 378-392.
8. McKinnon, J. J.; Jayatilaka, D.; Spackman, M. A., Towards quantitative analysis of intermolecular interactions with Hirshfeld surfaces. *Chem. Commun.* **2007**, 3814-3816.

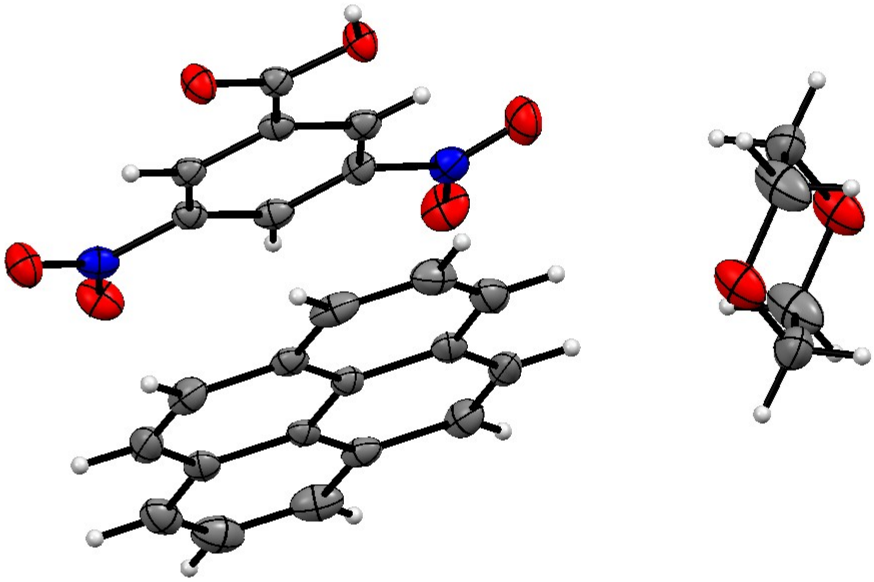

Fig. S1 *ORTEP* diagram (50% ellipsoid probablity) of cocrystal **1**.

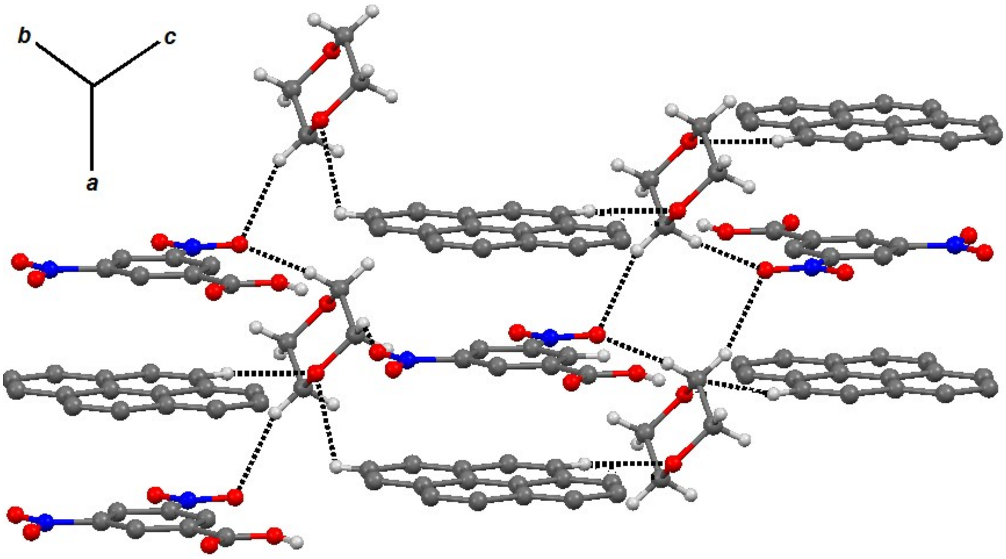

Fig. S2 1,4-dioxane interdigitates mixed 3,5-DNB:pyrene stacks forming multiple C−H···O hydrogen bonds.

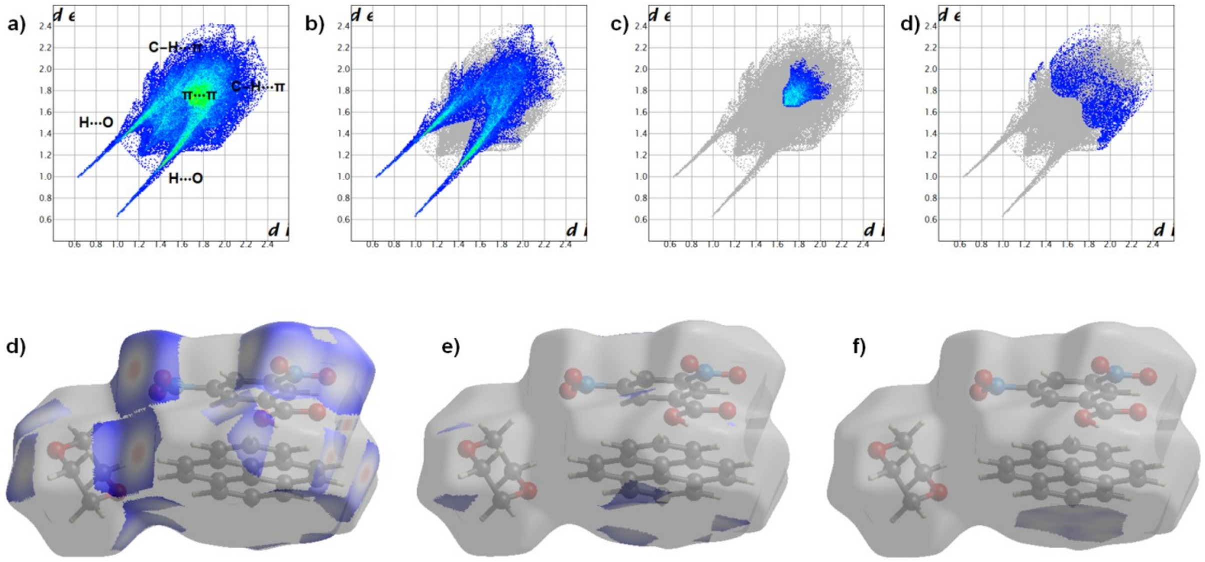

Fig. S3 a) 2D fingerprint plot showing all intractions in cocrystal **1**; b) 2D fingerprint showing O···H contact; c) 2D fingerprint plot showing C−H···π interaction; d) 2D fingerprint plot showing C−H···O interaction; e) 2D fingerprint plot showing O···H contact; f) *d_{norm}* surface showing C−H···π interaction; g) *d_{norm}* surface showing C−H···O interaction.

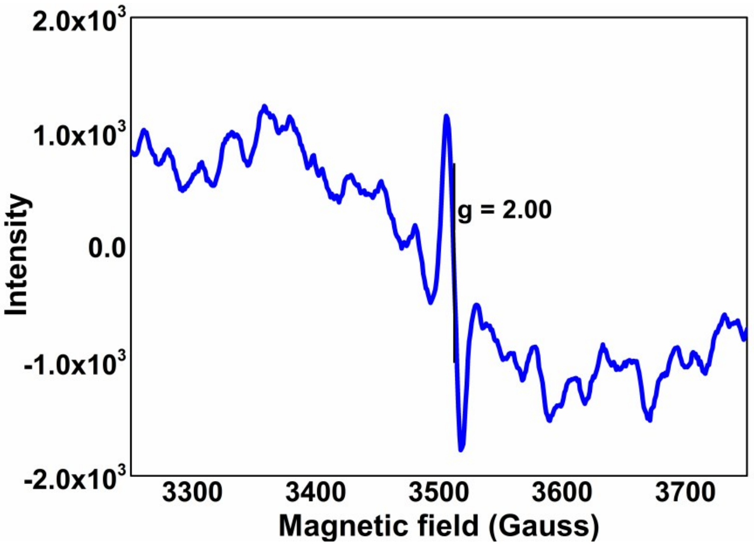

Fig. S4 EPR spectrum of cocrystal **1** shows weak signal with g = 2.002.

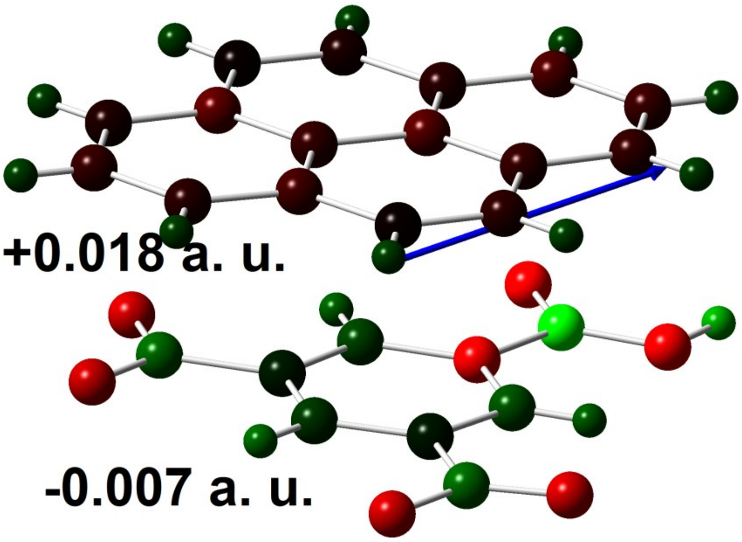

Fig. S5 Static dipole moment (SDM) and charge distribution on coformers manifest lower degree of charge transfer in cocrystal **1**.

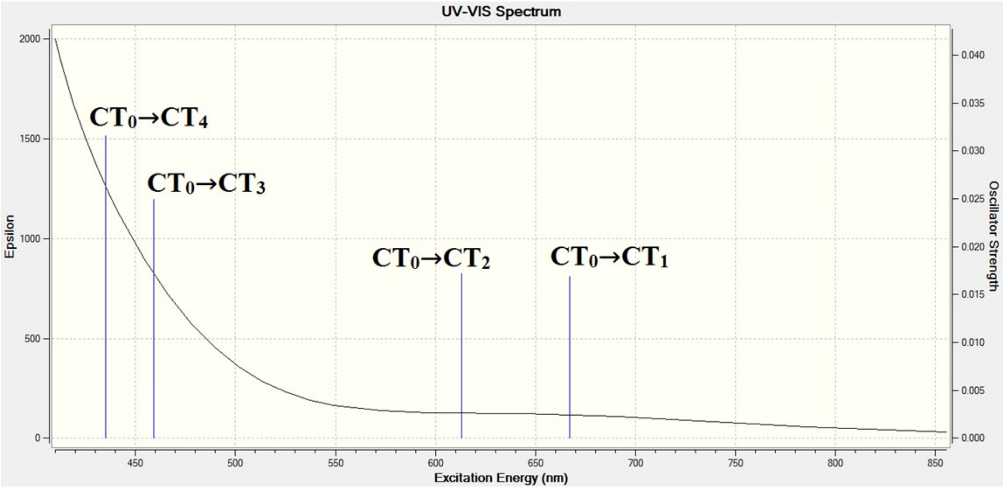

Fig. S6 Calculated UV-Vis spectrum of cocrystal **1** at B3LYP/6-311G(d,p) level of theory.

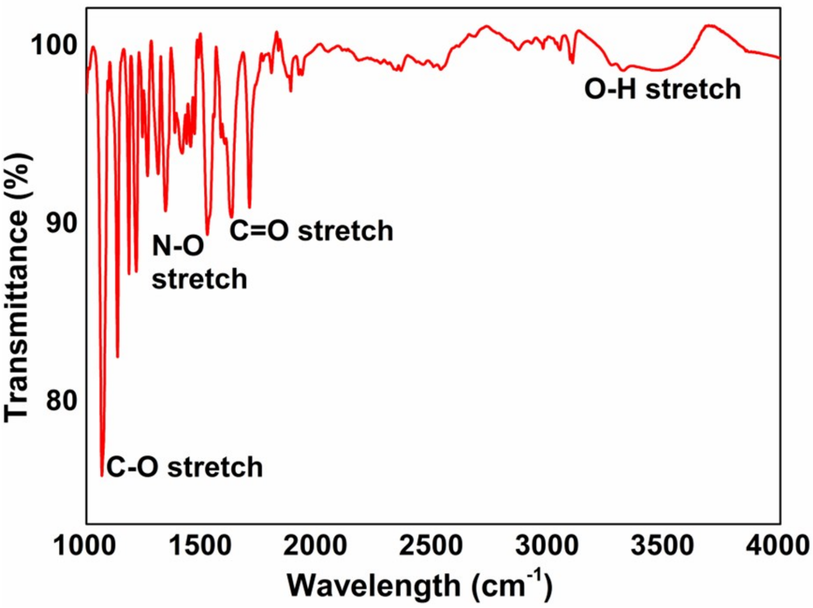

Fig. S7 FTIR spectrum of cocrystal **1** shows broad O−H stretching band indicating the presence of doubly hydrogen bonded 3,5-DNB dimer.

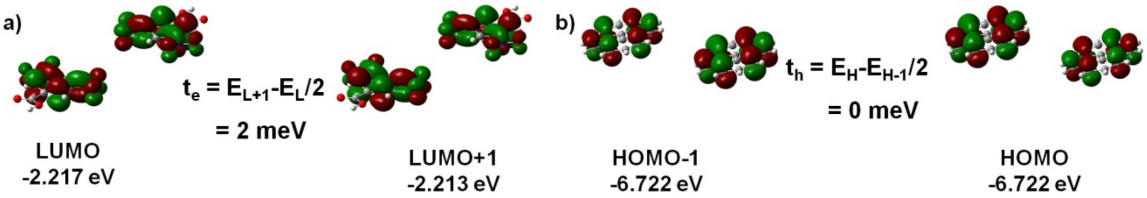

Fig. S8 Direct electron and hole transfer integrals of cocrystal **1**.

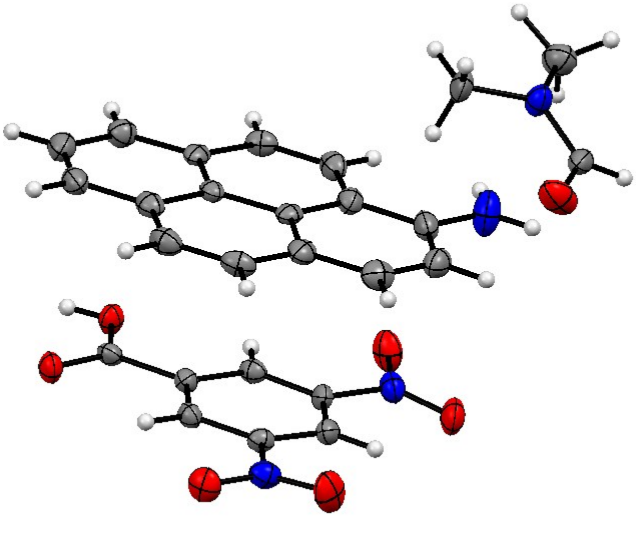

Fig. S9 *ORTEP* digram (50% thermal elliposoid probablity) of cocrystal **2**.

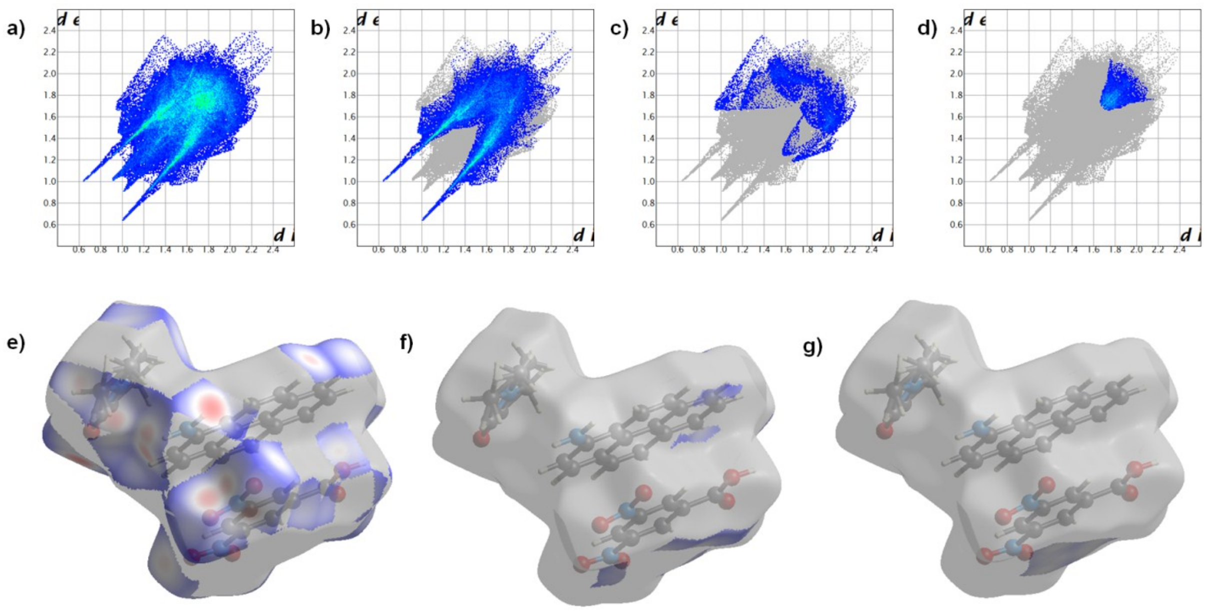

Fig. S10 a) 2D fingerprint plot showing all intractions in cocrystal **2**; b) 2D fingerprint showing O···H contact; c) 2D fingerprint plot showing C−H···π interaction; d) 2D fingerprint plot showing π···π interaction; e) d_{norm} surface showing O···H contact; f) d_{norm} surface showing C−H···π interaction; h) d_{norm} surface showing π···π interaction.

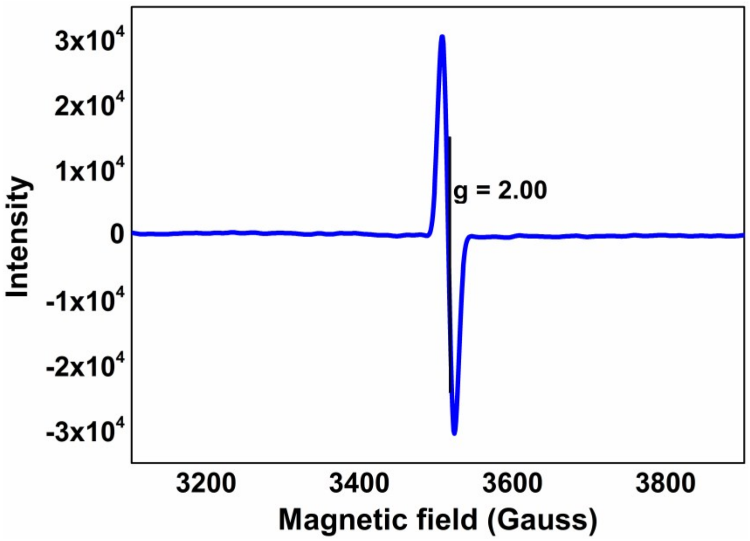

Fig. S11 EPR spectrum of cocrystal **2** shows a strong signal, however, 1-aminopyrene shows EPR signal due to presence of minor amount of 1-aminopyrene radical.

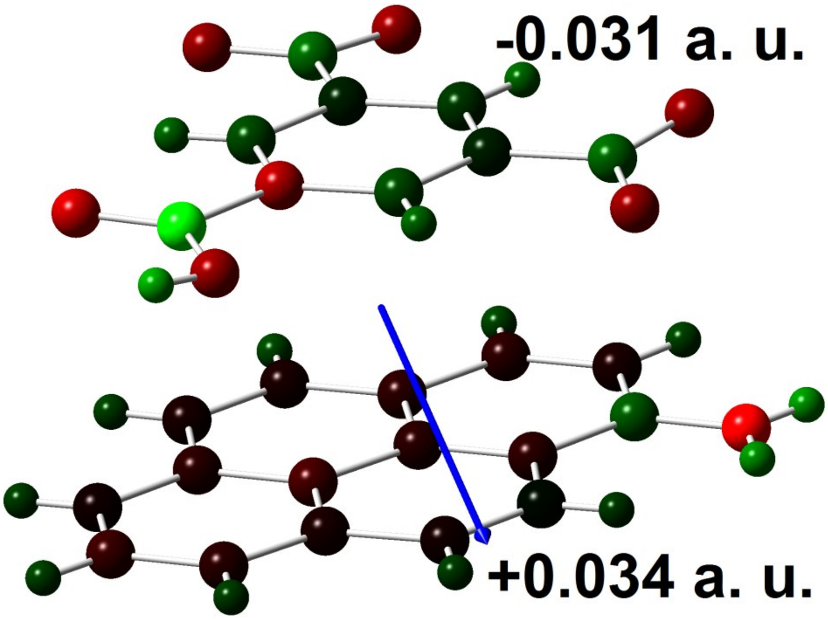

Fig. S12 Static dipole moment and charge distribution on the coformers indicate charge transfer in cocrystal **2**.

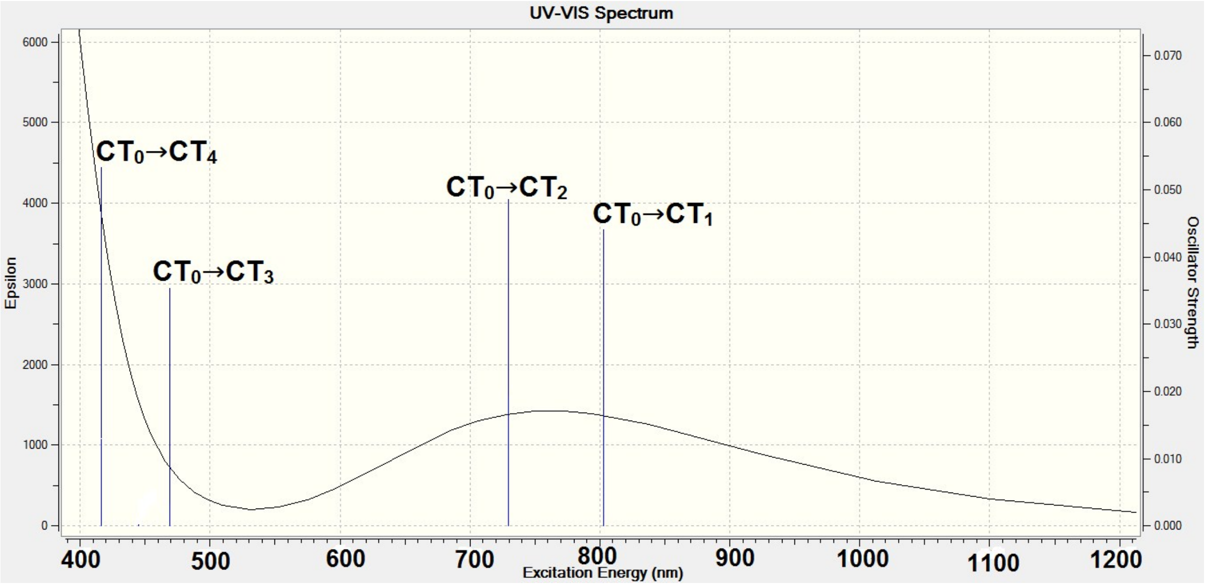

Fig. S13 Calculaed UV-Vis spectrun of cocrystal **2** showing CT$_0$→CT$_1$, CT$_0$→CT$_2$ and CT$_0$→CT$_3$ electronic transitions.

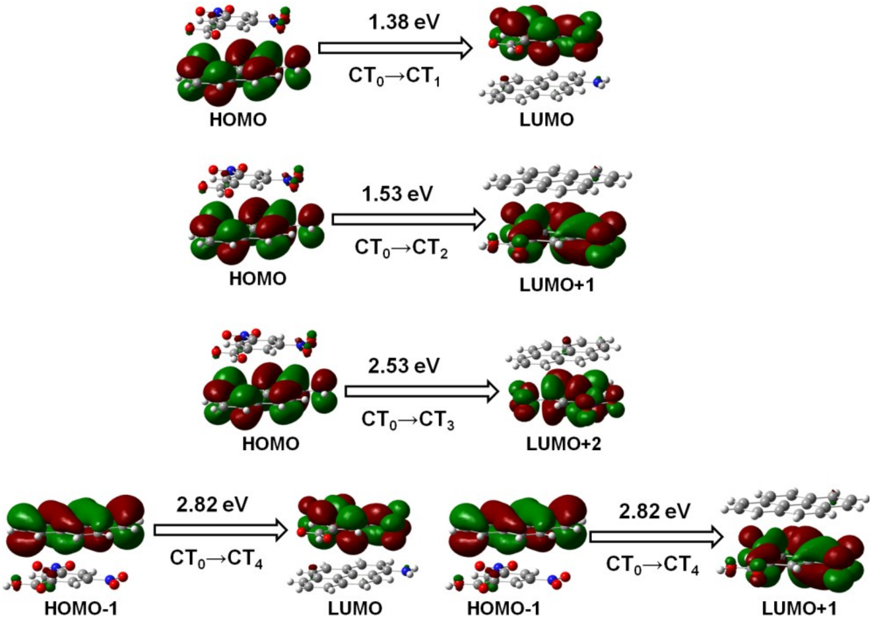

Fig. S14 Molecular orbitals taking part in electronic transition in cocrystal **2**.

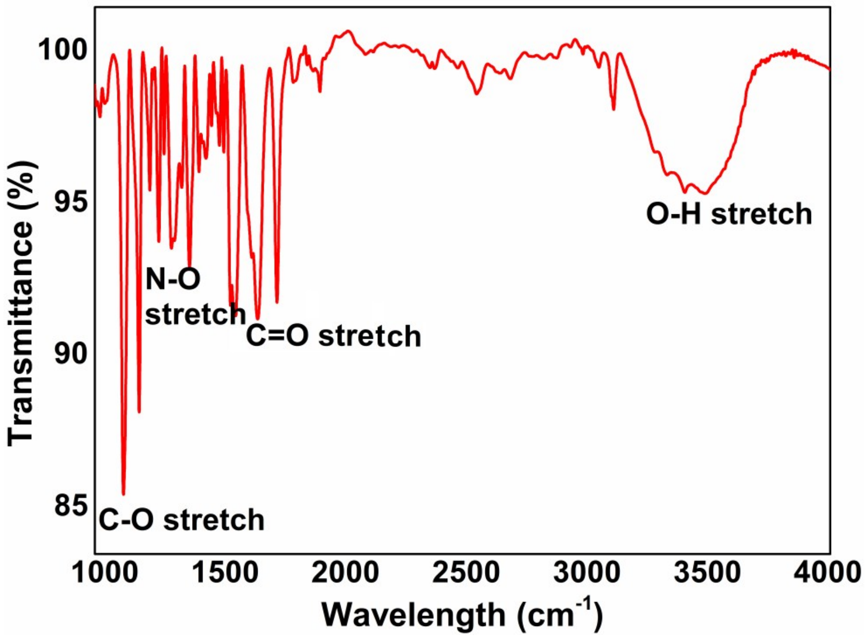

Fig. S15 FTIR spectrum of cocrystal **2** shows broad O−H stretching band which merges with N−H stretching band.

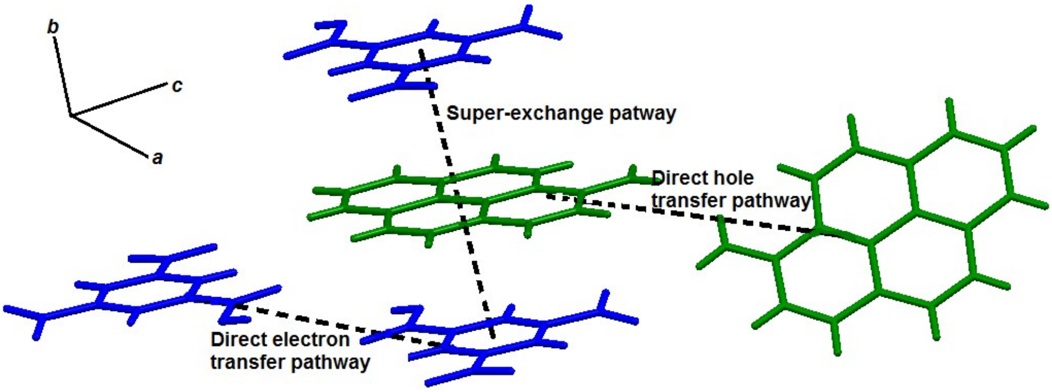

Fig. S16 Super-exchange and direct charge transfer pathways in cocrystal **2**.

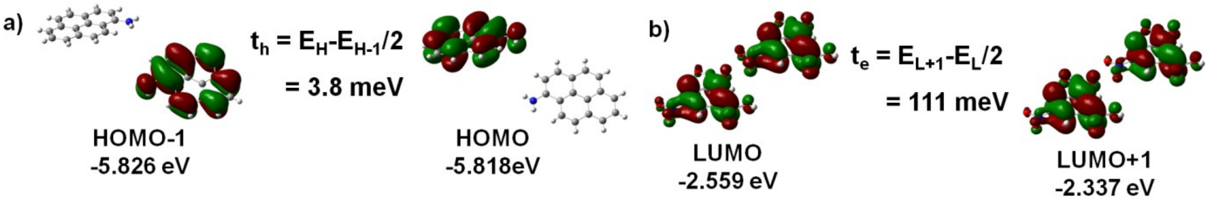

Fig. S17 Direct charge transfer integrals in cocrystal **2**, all calculated at CAM-B3LYP/6-311G(d,p) level.

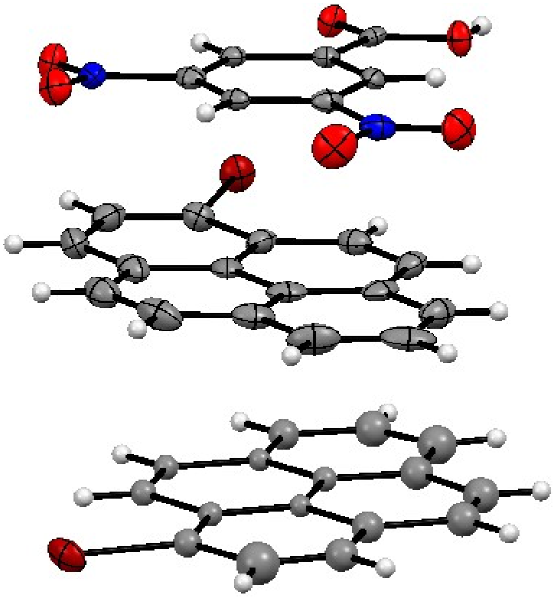

Fig. S18 *ORTEP* diagram (50% thermal ellipsoid probablity) of cocrystal **3**, thermal ellipsoids are not shown for disordered 1-bromopyrene molecue.

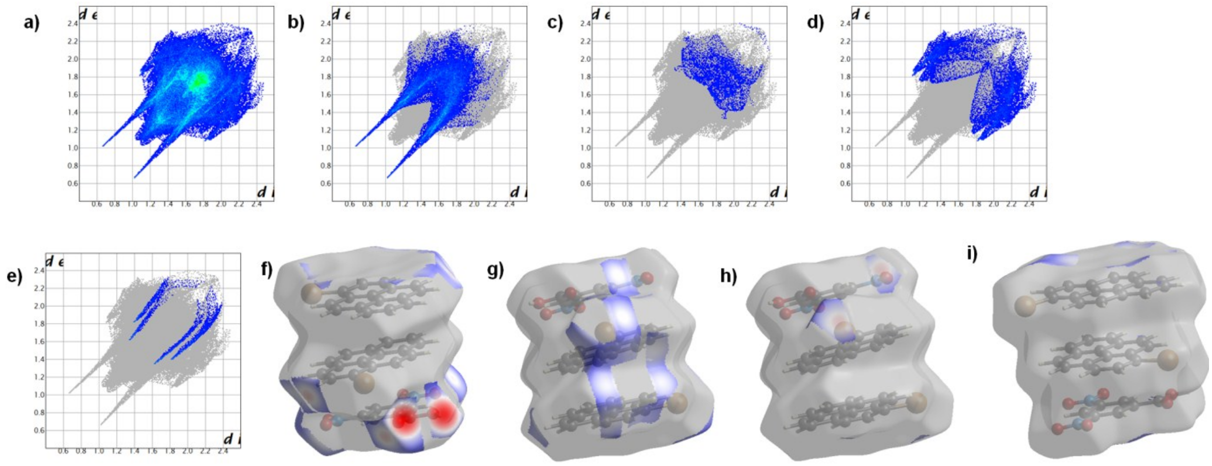

Fig. S19 a) 2D fingerprint plot showing all intractions in cocrystal **3**; b) 2D fingerprint showing O···H contact; c) 2D fingerprint plot showing C−H···π interaction; d) 2D fingerprint plot showing C−H···Br interaction; e) 2D fingerprint plot showing Br···O interaction; f) d_{norm} surface showing O···H contact; g) d_{norm} surface showing C−H···π interaction; h) d_{norm} surface showing C−H···Br interaction; i) d_{norm} surface showing Br···O interaction.

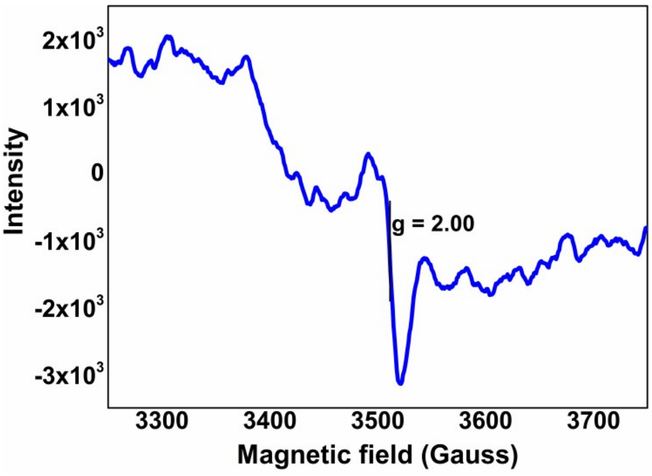

Fig. S20 EPR spectrum of cocrystal **3** showing weak signal with g = 2.002.

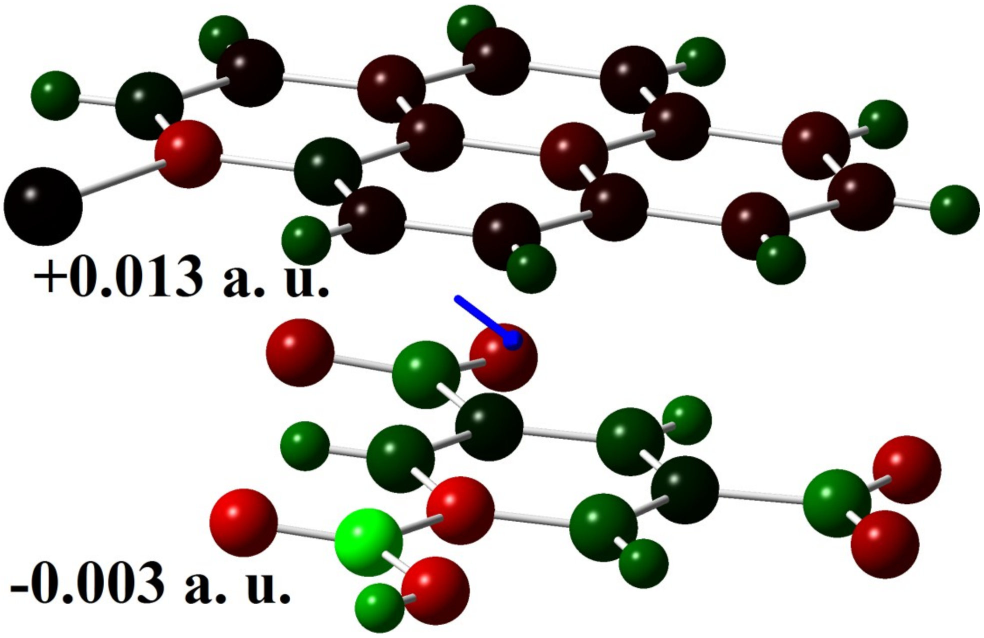

Fig. S21 Static dipole moment (SDM) and charge distribution on coformers of cocrystal **3** confirms charge transfer.

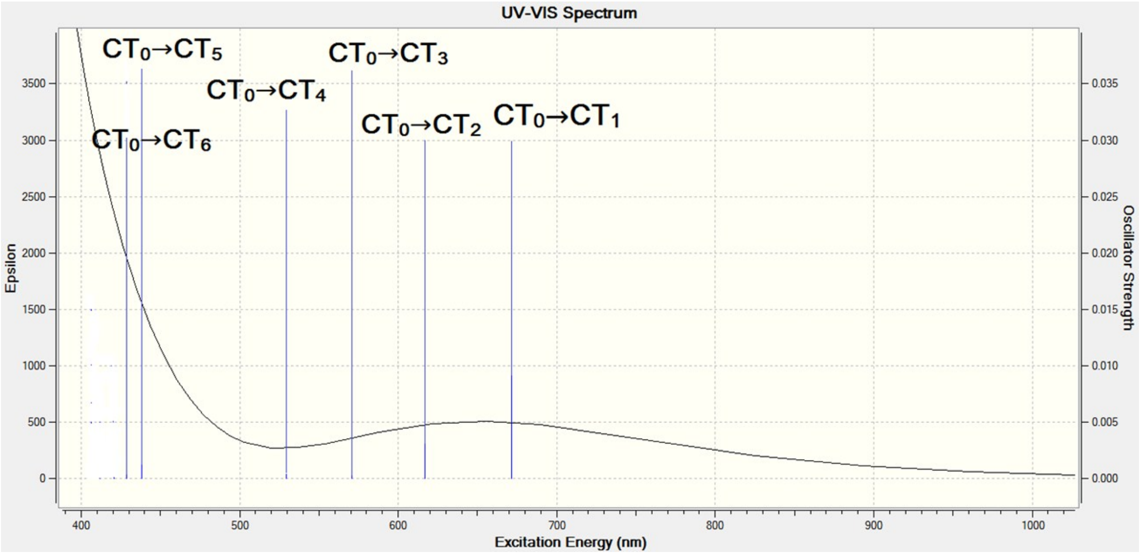

Fig. S22 Calculated UV-Vis spectrum of cocrystal **3** at B3LYP/6-311G(d,p) level.

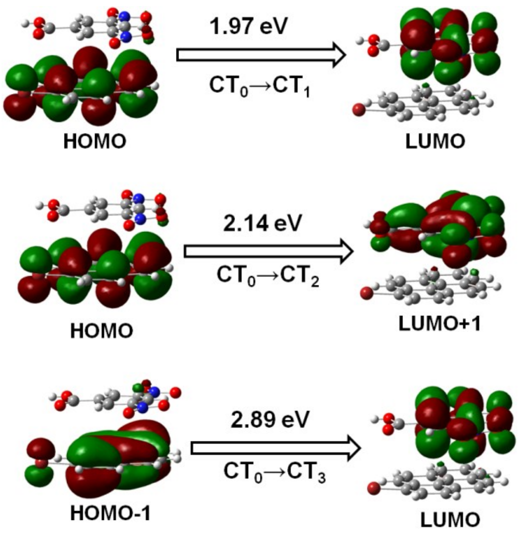

Fig. S23 Molecular orbitals taking part in electronic transition of cocrystal **3**.

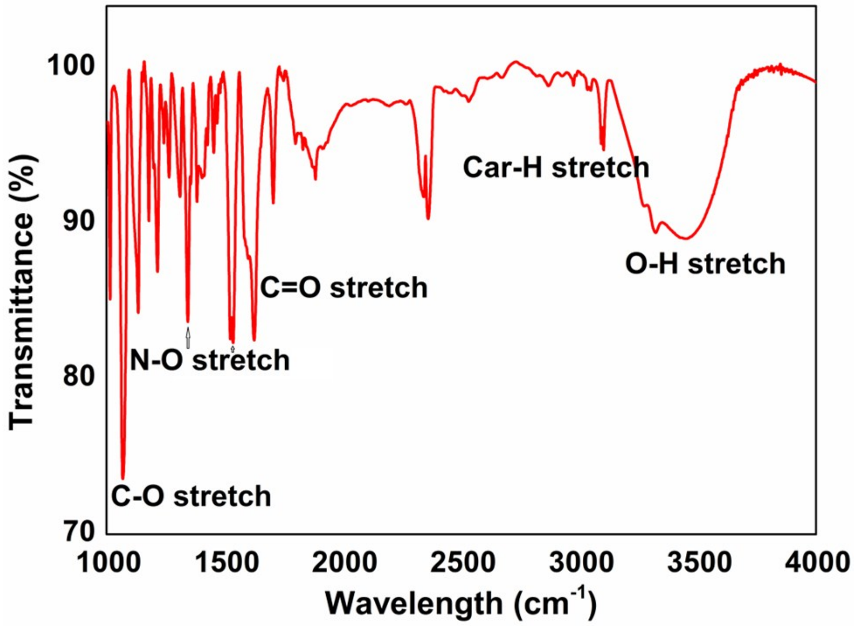

Fig. S24 FTIR spectrum of cocrystal **3**.

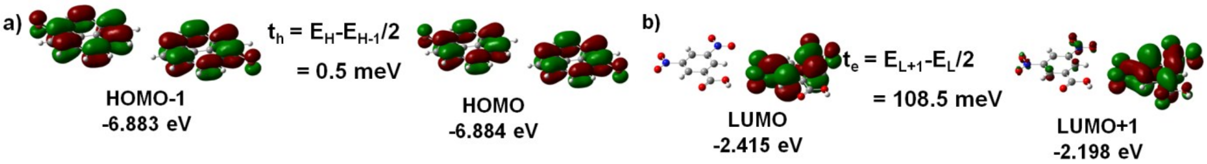

Fig. S25 Direct electron and hole transfer transfer integrals in cocrystal **3**, all calculated at CAM-B3LYP/6-311G(d,p) level.

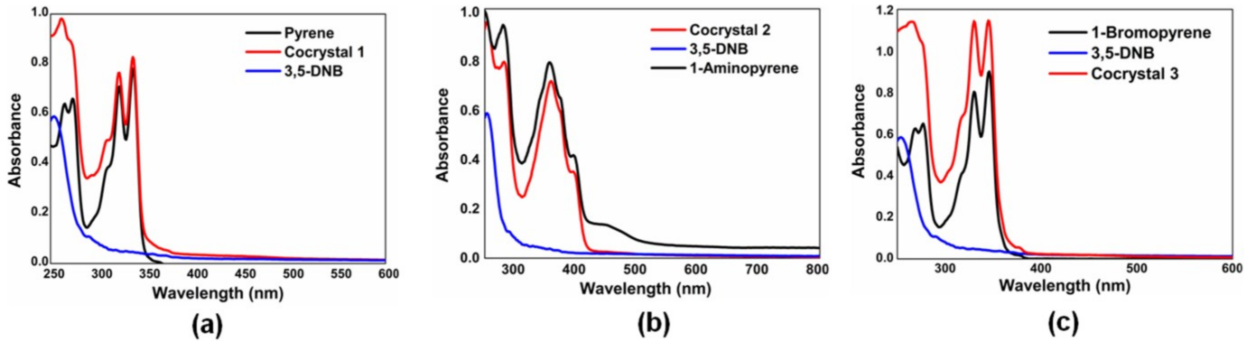

Fig. S26A UV-Vis spectra of cocrystals **1**-**3**.

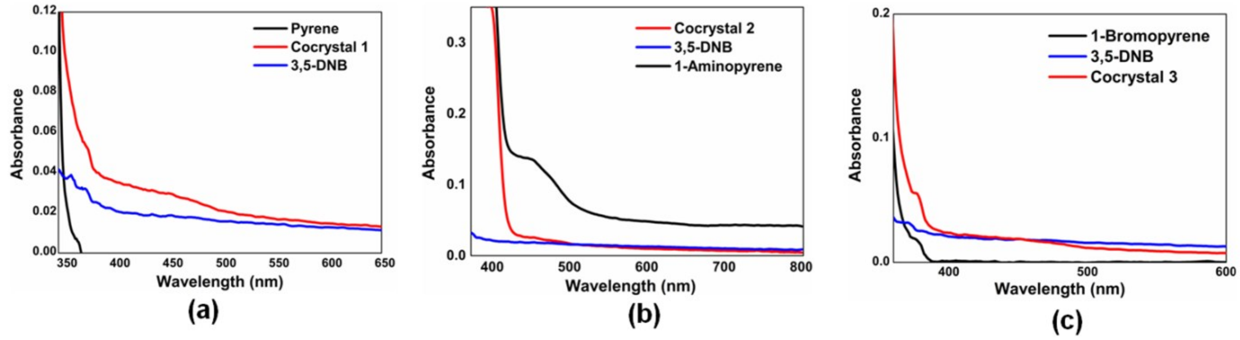

Fig. S26B UV-Vis spectra of cocrystals **1**-**3** highlighting the charge transfer region.

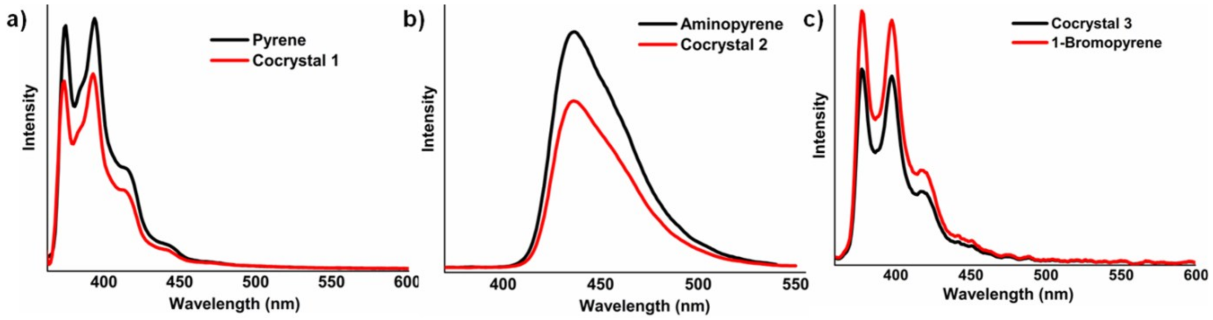

Fig. S27 Fluorescence spectra of cocrystals **1**-**3** and corresponding π-donors in chloroform solution.

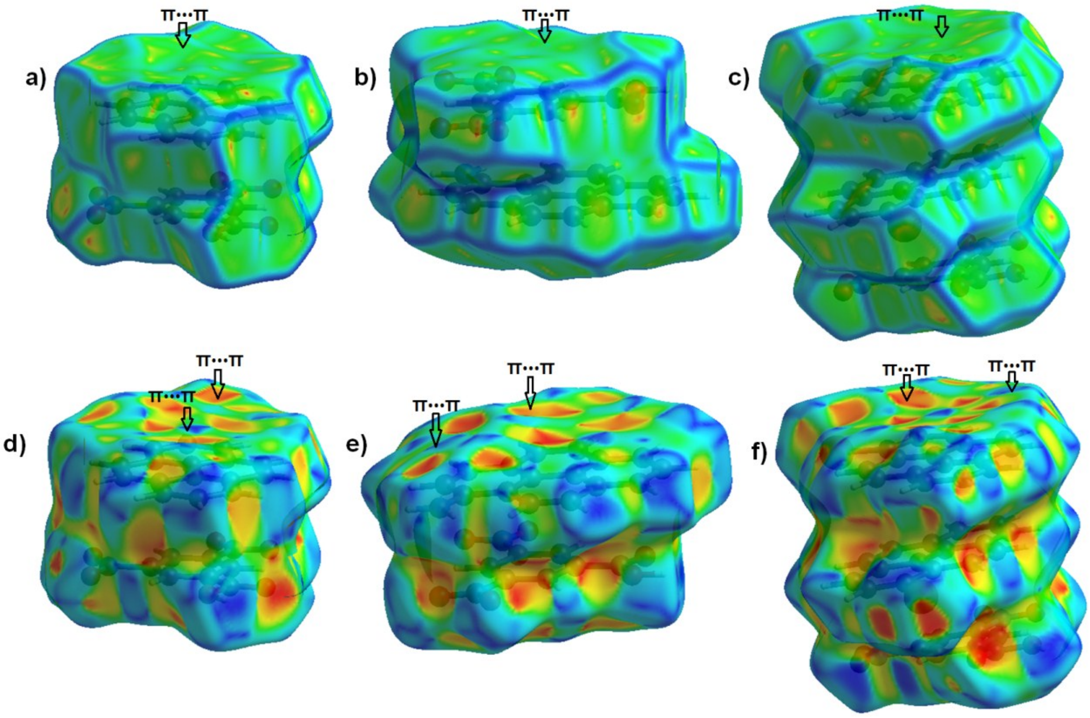

Fig. S28 a) Curvedness plot of cocrystal **1**; green and blue regions exhibit flat and regions with positive curvatures; b) Curvedness plot of cocrystal **2**; c) curvedness plot of cocrystal **3**; d) Shape index plot of cocrystal **1**, red: convex, green: region at saddle point and blue: concave; e) Shape index plot of cocrystal **2** with green and magenta regions indicating π···π stacking; f) Shape index plot of cocrystal **3** showing green and magenta regions corresponding to π···π stacking.

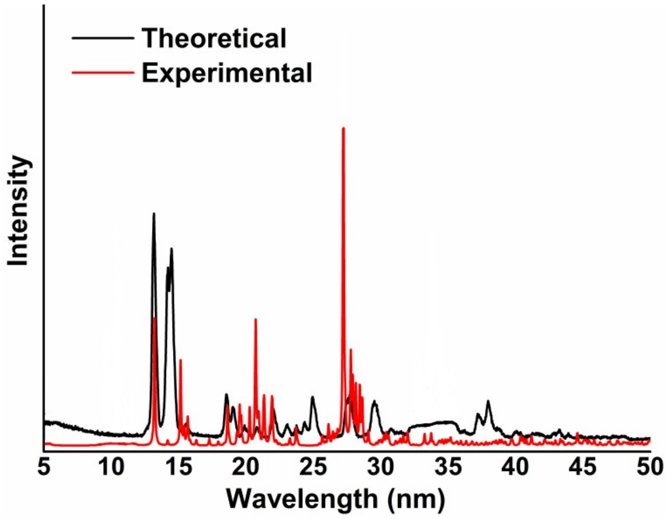

Fig. S29 PXRD pattern of cocrystal **1**.

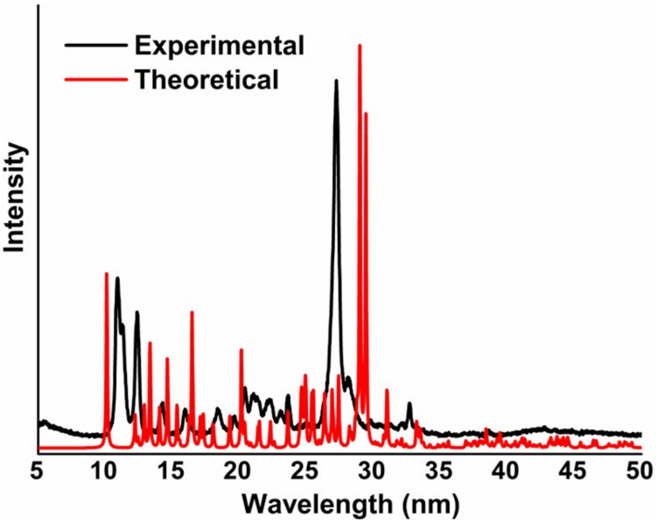

Fig. S30 PXRD pattern of cocrystal **2**.

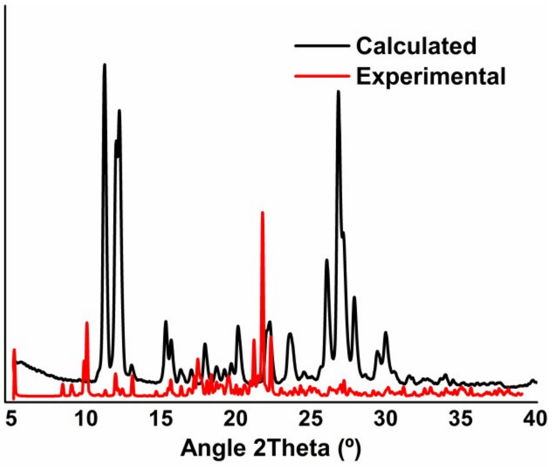

Fig. S31 PXRD pattern of cocrystal **3**.